Biomass Conversion and Biorefinery
https://doi.org/10.1007/s13399-023-04937-9

ORIGINAL ARTICLE

Production of phenolic compounds from argan shell waste by reductive catalytic fractionation

Zainab Afailal[1] · Noemí Gil-Lalaguna[1] · Martin Høj[2] · Alfonso Cornejo[3] · José Luis Sánchez[1] · Anker Degn Jensen[2]

Received: 6 July 2023 / Revised: 12 September 2023 / Accepted: 20 September 2023

Abstract
For efficient utilization of lignocellulosic biomass components, reductive catalytic fractionation appears as a promising biorefinery strategy. In this work, this concept of biomass valorization was used to study the potential of an unexplored feedstock, argan shells. This material was processed in a non-catalytic route and over a Pd/C catalyst in two different reaction media. The effects of the treatment temperature (250, 275, and 300 °C), as well as the catalyst loading (catalyst/argan shells mass ratio of 0.05 and 0.1 g/g), were also studied. The main product (lignin-derived oil) was thoroughly characterized using GC/MS/FID, SEC, and NMR. The highest monomer yields of 48–49 wt% based on the lignin content were obtained for n-butanol/water reaction medium at 300 °C using a Pd/C catalyst load of 0.1 g/g and for methanol reaction medium at 275 °C and 0.05 g/g. Significantly lower monomeric phenol yields were obtained in the non-catalytic route (4–19 wt% for n-butanol/water and 9–16 wt% for methanol). The main phenolic monomers in the catalytic pathway were 4-n-propanolguaiacol, 4-n-propanolsyringol, and 4-alkyl guaiacols and syringols, with some differences in the selectivities from one solvent to another.

Keywords Argan shells · Agricultural waste · Native lignin · Reductive catalytic fractionation · Hydrogenolysis

1 Introduction

Replacing fossil-based products with more sustainable resources, such as lignocellulosic biomass, for the production of fuels, chemicals, and materials has become a worldwide challenge [1]. In the past 50 years, the obtention of chemicals and biofuels from lignocellulose has mainly focused on converting the carbohydrate fraction, leaving behind the lignin as a subordinate constituent [1–3]. Lignin is a biopolymer with a complex structure composed of phenyl propanoid groups, guaiacyl, syringyl, and hydroxyphenyl, linked through ether and C-C bonds [4, 5]. Many processes can isolate lignin from the lignocellulosic biomasses, such as the kraft, sulfite, organosolv, and soda pulping processes [6]. However, the obtained lignin, also called technical lignin, differs in structure from native lignin [7–9] due to the condensation reactions occurring after the cleavage of the ether and ester bonds and their substitution by more stable C-C bonds that render technical lignin more recalcitrant than native lignin [1]. Therefore, depolymerizing technical lignin is an even more challenging issue [9].

The reductive catalytic fractionation (RCF) appears as a promising pathway on the lignin extraction and conversion in the biorefinery community [10]. This methodology combines biomass fractionation with lignin solubilization (solvent-based under a hydrogen atmosphere), depolymerization, and stabilization [2, 3]. These hydrogenolysis reactions are performed in the presence of a transition metal-based catalyst.

Most RCF studies have used woody materials as feedstock, such as those published by Sels et al. [2, 7, 11] and Rinaldi et al. [12–14]. Concerning herbaceous biomasses, Anderson et al. studied the performance of corn stover in RCF [15], while a recent study involved wheat straw [16].

✉ Zainab Afailal
zainabafailal@unizar.es

[1] Thermochemical Processes Group, Aragón Institute of Engineering Research (I3A), Universidad de Zaragoza, C/ Mariano Esquillor s/n, 50018 Zaragoza, Spain

[2] Department of Chemical and Biochemical Engineering, Technical University of Denmark, Anker Engelunds Vej 1, Building 101A, 2800 Kgs. Lyngby, Denmark

[3] Institute for Advanced Materials and Mathematics (InaMat2), Department of Sciences, Universidad Pública de Navarra, 31006 Pamplona, Spain

Published online: 29 September 2023

Many catalysts have been tested in RCF, such as Pd/C [17], Ru/C [18], Ni/C [14], and Ni-Al_2O_3 [7]. The catalyst choice principally affects the product selectivity: arylpropanes are the main products when Ru is used, and arylpropanols in the case of Pd [1, 9, 17], even though the total oil yields are similar [17]. The solvent choice also has a significant role, especially in the delignification step. Schutyser et al. [19] studied, in the presence of a Pd/C catalyst, the effect of a large variety of bio-based solvents (within a wide polarity range) on the delignification degree and monophenolics yield.

Phenolic monomers can be used as precursors for many chemical products. For instance, Feghali et al. showed that depolymerized lignin oils (from woody biomass) enriched in phenolic hydroxyl groups were excellent bio-based substitutes for bisphenol A (BPA) in epoxy thermoset polymers [20, 21]. Furthermore, in a previous work from our research group [22], the production of antioxidants from the lignin contained in argan shells was evaluated through a two-step process: (i) lignin extraction via a semi-chemical pulping process and (ii) subsequent depolymerization under subcritical hydrothermal conditions. Argan shell is an unexplored agricultural waste generated in Morocco from production of argan oil, which is widely used as a cosmetic oil. Morocco produces over 4000 tons of argan oil annually, co-generating around 80.000 tons of non-valorized waste (shells) [23].

In the present study, the same waste, argan shells, underwent a one-pot conversion process based on RCF methodology in order to investigate and compare how the production of phenolic monomer compounds is affected by the conversion process. Up to date, and to the best of our knowledge, this methodology has only been applied to woody and herbaceous feedstocks, and no research works can be found in the literature concerning the use of fruit shell residues, which are rich in lignin, as feedstock. Hence, lignin extraction and depolymerization from argan shells were studied by RCF in order to fill the gap in the literature concerning the use of fruit shells. The degree of depolymerization and product selectivity has been evaluated in both a non-catalytic pathway and using Pd/C as a catalyst. This catalyst was chosen with the objective of maximizing the yield of phenolic monomers, while obtaining –OH functionalized alkyl chains for further applications. Detailed characterization was carried out to understand the effect of the operating conditions on product composition.

2 Materials and methods

2.1 Materials

Argan shells (AS) were collected in the region of Essaouira (southwest of Morocco, 31°30′ 47″ N, 9° 46′ 11″ W) by the summer of 2019. AS were kindly supplied by a woman cooperative after argan kernels extraction. This residue is characterized, as exposed in Table S1 in the Supporting Information section (SI), by a low ash content (0.3 wt%), low extractives content (0.2 wt%), and a high lignin content (34 wt%). AS was crushed and sieved in order to obtain a powder less than 200 µm in size.

2.2 Experimental setup and methodology

Two different series of experiments were performed depending on the reaction medium used: (i) 1:1 vol. n-butanol/water or (ii) pure methanol. In both cases, the RCF experiments were conducted in a stainless steel Parr reactor 4575 (Parker Inc. USA) operating in batch mode (Figure S1 in SI). In a typical run, 20 g of AS, together with Pd/C catalyst (0, 1 or 2 g), were suspended in 200 mL of the solvent. In this study, methanol and n-butanol/water mixture were compared as reaction mediums to investigate their extraction capacities as well as the effect of the solvent polarity in the RCF reaction. The reactor vessel was sealed and flushed first with N_2, then H_2. Finally, the system was pressurized to 26 bars with H_2 at room temperature. The reactor was heated up to the specified temperature (250, 275, or 300 °C) at a heating rate of up to 10 °C/min, and the final temperature was maintained for 2 h. Then, the reactor was cooled by immersing it in an ice bath. After room temperature was reached, a gas sample was collected in a Tedlar gas bag to be analyzed using a Thermo Scientific Trace 1300 gas chromatograph, pre-calibrated with an external standard. The gas yield (on H_2 and N_2 free-basis) was calculated according to Eq. 1. The remaining gas-phase was discharged by flushing the reactor with N_2 for 15 min. Once the reactor was open, the liquid and solid phases were gravimetrically quantified to determine the mass balance. A weighed amount of the same solvent used as reaction medium (n-butanol/water mixture or methanol) was used to wash the reactor and recover the sticky organic fraction remaining on the reactor stirrer, walls and cooling coils. The mixture of liquid, solid, and washing solvent was filtered (with additional flushing of the filter cake using the same solvent). The filtered solid was dried in a Büchner funnel under vacuum for at least 4 h (with a flow of N_2 on the top of the Büchner funnel, as shown in Figure S2 in the SI, to prevent possible autoignition of the spent catalyst (Pd/C) with the adsorbed hydrogen [24]), and then left overnight in a desiccator under vacuum. The dried solid was weighed, and the solid yield was calculated according to Eq. 2.

$$\text{Gas yield (wt\%)} = \frac{\sum m_{g-GC}}{W_{AS}} \cdot 100 \quad (1)$$

$$\text{Solid yield (wt\%)} = \frac{W_S - W_{Cat}}{W_{AS}} \bullet 100 \quad (2)$$

where $m_{g\text{-}GC}$ is the mass of each individual gas compound quantified through GC, W_S is the weight (g) of the dried filtered solid, W_{Cat} is the weight (g) of the Pd/C loaded in the reactor, W_{AS} is the weight (g) of the AS fed (as-received basis).

In the n-butanol/water-experiments, the two immiscible phases of the filtrate were separated using a decantation funnel. Three aliquots from the organic phase were dried for 18 h at 117 °C (boiling point of n-butanol) to determine the corresponding yield of n-butanol-soluble oil (BSO) according to Eq. 3.

Because of the higher temperature required for removing n-butanol, other volatile compounds, apart from butanol, can be lost during the drying stage. In order to quantify such losses, another aliquot from the organic phase was distilled at the softest conditions in a rotary evaporator (60 °C and 150 mbar) to separate the lightest organic compounds from the heaviest n-butanol soluble oil (n-butanol could not be evaporated at 150 mbar and 60 °C) and to estimate the organic volatiles losses during the drying process.

Subsequently, the previously decanted aqueous phase was extracted with 50 mL of n-butanol and then separated again to extract the remaining depolymerized lignin products. After this second extraction, aliquots from the two phases were dried for 18 h at 105 °C and 117 °C to evaporate water and n-butanol, respectively, resulting in two more fraction products: RAP (remaining in the aqueous phase) and EAP (extracted from aqueous phase).

No separation or extraction steps were performed in the runs where methanol was used as the reaction medium. In this case, the filtered liquid was the unique liquid product, which was dried during 18 h at 70 °C to determine the yield of methanol-soluble oil (MSO).

$$\text{BSO/MSO yield (wt\%)} = \frac{X_{DO} \cdot W_{OF}}{W_{AS}} \bullet 100 \quad (3)$$

where W_{OF} is the weight (g) of the filtered organic liquid collected in each experiment, X_{DO} is the content of dried matter (MSO or BSO) in this filtered liquid (wt%, determined in the drying procedure), and W_{AS} is the weight (g) of the AS fed (as-received basis). Note that only the AS weight was considered in the yield calculation. The possible reaction between the solvent and the biomass was not considered, as the products of these reactions were evaporated during the drying step.

2.3 Experimental design

A full factorial experimental design 2^k with two factors and two levels was established for each reaction medium (n-butanol/water and methanol) in order to evaluate the effect of both the temperature (250–300 °C) and the catalyst loading (0–2 g, corresponding to a catalyst/AS mass ratio of 0.0 to 0.1 g/g) on the yields and the characteristics of the produced oils. To evaluate the experimental error, three replicates at the central point of the factor levels were conducted (for each reaction medium). Hence, a total of 14 experiments were performed (Table 1). The experimental results were evaluated through an analysis of variance (ANOVA) with a confidence level of 95%, including the following response variables: (i) product distribution: solid, gas, and oil yields, differentiating between the production of lignin-monomers and carbohydrate-fraction in the oil; (ii) characterization of the oils, including the results of the average molecular weight, the composition determined by gas chromatography, and nuclear magnetic resonance spectroscopy (NMR).

2.4 Product characterization

The filtered organic liquids (MSO and BSO including the light fraction, that is, before drying) were analyzed by gas chromatography (GC) with an Agilent 7890A GC chromatograph equipped with a flame ionization detector (FID) and combined with an Agilent 5975C mass selective detector (MSD). Compound identification and quantification were performed based on the peaks with more significant areas (up to 88 % of the total FID area was quantified). The FID signal (used for the quantification) was calibrated for the phenolic compounds (guaiacol, creosol, 2,4,6-trimethylphenol, phenol, 4-ethylguaiacol, 2,5-dimethylphenol, p-cresol, eugenol, 4-ethylphenol, syringol, 3-methoxycatechol, 4-allylsyringol, vanillin, apocynin, guaiacylacetone,

Table 1 Experimental conditions in the RCF tests (2^k full factorial design)

Exp. no.	Reaction medium	*T* (°C)	Pd/C amount (g)
1	n-Butanol/water (1:1 vol.)	250	0
2		300	0
3		250	2
4		300	2
5		275	1
6		275	1
7		275	1
8	Methanol	250	0
9		300	0
10		250	2
11		300	2
12		275	1
13		275	1
14		275	1

homovanillyl alcohol, orcinol, catechol, hydroquinone) using 8 standard solutions with concentrations ranging between 50 and 3000 µg/mL. For the carbohydrate-derived compounds, 5 standard solutions (1,2 propanediol, 2-cyclopenten-1-one, 2-ethyl-1-hexanol, furfural, ethylene dimethcrylate, n-butyl acetate, furfuryl alcohol, 2,5-dimethylfuran) with concentrations ranging between 100 and 5000 µg/mL were prepared. All the standards were prepared using dichloromethane-methanol (1:1 vol.) as solvent. Finally, a commercial standard (Supelco 37 Comp. FAME mix) was used to calibrate the FID signal for fatty acid methyl esters (FAME) and other aliphatic esters. The "relative response factor" based on the effective carbon numbers (ECN) methodology [25, 26] was applied to determine the concentration of the compounds identified by MSD but not present in the aforementioned standards. More information about the operating parameters, standards, calibration, and ECN calculation can be found in Table S2 and S3 in the SI.

The phenolic monomer yields (for some specific compounds and as a total phenolic fraction) were calculated from GC/MS/FID data (Eq. 4). Similarly, the individual and total yields of carbohydrate-derived compounds (furan, alcohols, C5 and C6 ketones, linear esters, and ethers) were calculated using the GC/MS composition data (Eq. 5).

$$Y_{\text{Monomers}}\ (\text{wt\%}) = \sum \left(\frac{m_{\text{i-GC}}}{W_{\text{AS}}} \right) \bullet 100 \tag{4}$$

$$Y_{\text{carbohydrate-derived}}\ (\text{wt\%}) = \sum \left(\frac{m_{\text{j-GC}}}{W_{\text{AS}}} \right) \bullet 100 \tag{5}$$

where $m_{\text{i-GC}}$ is the individual mass of each phenolic monomer identified and quantified through GC/MS/FID and $m_{\text{j-GC}}$ is the individual mass of each carbohydrate-derived compound determined through GC/MS/FID and W_{AS} is the weight (g) of the AS fed (as-received basis).

The molecular weight distribution of BSO and MSO was measured via size exclusion chromatography (SEC). The measurements were performed with an Agilent 1100 HPLC using two coupled HR-5 and HR-1 Styragel (Waters) columns as the stationary phase at 30 °C and two detectors, UV-vis detector and refractive index detector (RID), with tetrahydrofuran (THF) as mobile phase. The samples were dissolved in the eluent with a concentration of 10 mg/mL in THF; 25 µL of the sample was injected for each analysis at an elution flow rate of 1 mL/min. The wavelength of 254 nm in the UV-visible detector is principally suitable to detect the aromatic species; however, the RID detector detects, in addition to the aromatics, other compounds such as the saccharides and compounds from solvent (methanol and n-butanol) degradation. The molecular weight was calibrated against the retention time, as reported in [27].

NMR measurements were made at 300 K on a Bruker Ascend III spectrometer equipped with a PABBO 5 mm probe at 400 MHz and 101 MHz for ^{1}H and ^{13}C, respectively, and were processed using the Bruker Topspin 3.6.2 software. NMR samples were prepared in DMSO-d_6 and referenced using the residual signal at 2.50 ppm and 39.52 ppm for ^{1}H and ^{13}C measurements [28]. More details about NMR characterization can be found in the SI.

3 Results and discussion

3.1 Product distribution

The mass balance in most of the experiments closed between 90 and 99 % (calculated directly from the mass of reactants loaded into the reactor and the products mixture recovered just after the reaction, before the separation procedure). The one-pot conversion of argan shells into oil and gas (calculated as 100 % minus the solid yield) widely ranged depending on the operational conditions: 79–97 % for n-butanol/water-experiments and 33–89 % for methanol-experiments.

Figure 1 summarizes the product distribution in each experiment, including most of the fractions recovered and quantified. The sum of the product yields does not fit with the overall mass balance because of the volatiles lost during the drying stage required for removing the solvent and

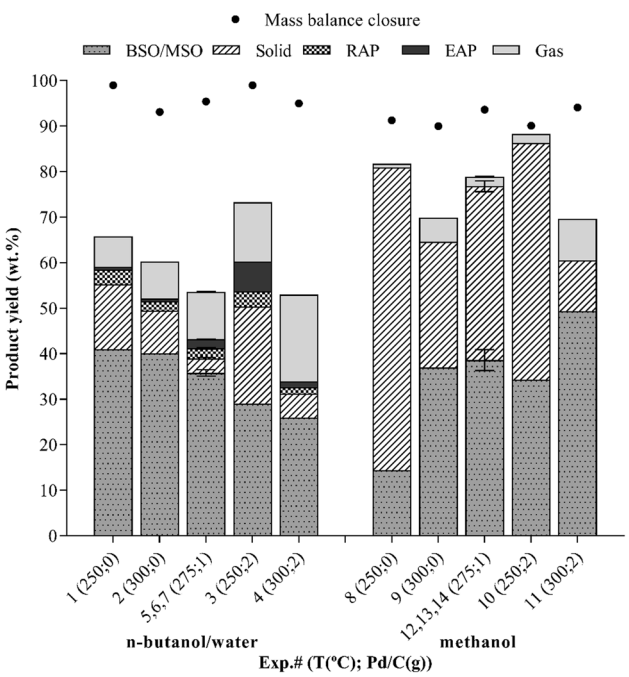

Fig. 1 Summary of the product distribution in RCF experiments: RAP, remaining in the aqueous phase; EAP, extracted from aqueous phase

quantifying the MSO or BSO yields. This difference was more pronounced in the case of n-butanol/water-experiments than in methanol-experiments as a consequence of the higher evaporation temperature (117 °C for n-butanol and 70 °C for methanol). According to the estimation of these losses obtained in the distillation procedure, the light fraction (volatiles) in the organic phase of n-butanol/water-experiments ranged between 28 and 40 wt%, which matches with the missing fraction to close the mass balance. For this reason, the GC/MS/FID characterization was carried out on the filtered organic liquids (samples before drying) to gain insight into the nature of the volatiles in this fraction.

For a better understanding and interpretation of the experimental results, Fig. 2 plots the ANOVA of the yields of solid, gas and oil (BSO or MSO) (error bars correspond to the least significant difference at a confidence level of 95 %). As can be seen, the increase of the treatment temperature from 250 to 300 °C significantly reduced the amount of remaining solid, regardless of the catalyst load or reaction medium. Furthermore, less solid was obtained when using the mixture of n-butanol/water (Fig. 2a) compared to the use of methanol (Fig. 2b). On the other hand, the highest Pd/C load minimized the solid yield to 11 % when using methanol (300 °C; 2 g Pd/C) (both factors, temperature and catalyst load, affected the solid yield in a linear trend with no interaction between them). The lowest solid yield when using the n-butanol/water mixture was only 3 % at the central point (275 °C; 1 g Pd/C), pointing to a significant interaction between the factors and a non-linear trend. Surprisingly, in this solvent, the solid yield obtained at 250 °C increased from 14 % in the non-catalytic condition to 21 % with catalyst.

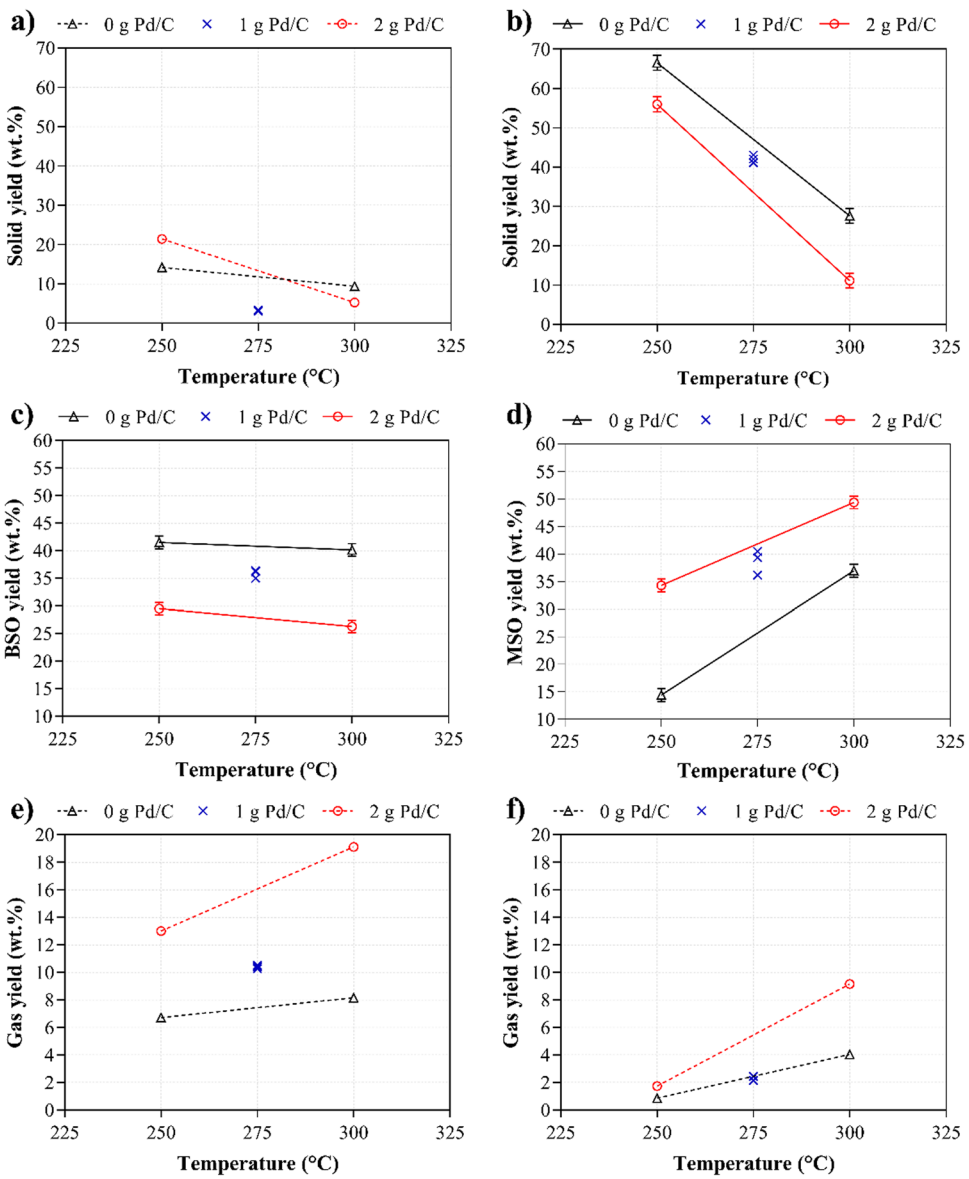

Fig. 2 Effect of temperature and catalyst loading on the product yields (solid, oil, and gas) when using n-butanol/water (**a**, **c**, **e**) and methanol (**b**, **d**, **f**) as reaction mediums

As shown in Fig. 2c and d, higher oil yields were obtained in the catalytic methanol pathway. The ANOVA shows that both the temperature and the catalyst load positively affected, in a linear trend, the production of MSO. However, for n-butanol/water, the presence of catalyst adversely affected BSO production, dropping from 40 wt% in non-catalytic conditions (Exp.#1 and #2) to around 26 wt% in the catalytic tests (Exp.#3 and #4) regardless of the reaction temperature. A similar trend was reported in the literature [29] when processing beech wood in ethanol at 300 °C over sulfided NiMo/ɣ-Al_2O_3, where the oil yield decreased from 50 wt% (non-catalytic process) to 44 wt% (in the presence of catalyst). That could be explained by the fact that using the catalyst caused a more significant fractionation, producing more volatiles (higher gas release) and decreasing the oil yield. The effect of the temperature on the recovered fraction of oil was much more significant when using methanol. Saccharides may be partially responsible for this difference in the effect of the temperature. It is well known that the decomposition of holocellulose to produce saccharides is promoted when increasing the temperature [29]. Since no phase separation was made in the case of using methanol (being a one-phase system), the increased fraction of saccharides remained in the MSO and contributed to increase its yield. However, when the reaction was performed in n-butanol/water, part of these saccharides was solved in the aqueous phase and the other part figured as a light organic fraction in the BSO that was evaporated in the drying process at 117 °C, therefore, were not included in the BSO yield, leading to a more or less constant BSO yield with the temperature.

On the other hand, the gas yield (Fig. 2e and f) was affected by both the temperature and the catalyst load in a non-linear trend for both reaction media. More gas was produced when using the catalyst, with maximal yields of 9 wt% and 19 wt% at 300 °C and 2 g of Pd/C in methanol and n-butanol/water, respectively. Table S4 in the SI exposes the gas composition obtained in each experiment (vol.% on a H_2 and N_2 free-basis). Essentially, in the non-catalytic conditions for both solvents, CO_2 was the main component in the produced gas (up to 90 vol.% in the case of n-butanol/water and 56 vol.% in the case of methanol). This trend changed when introducing Pd/C to the reaction medium, and CO became the principal produced gas (more than 60 vol.% in most cases) with a significant increase of CH_4 and C_2H_6 concentrations. This trend could be explained by the decarbonylation reactions of the released carboxylic acids, promoted by the Pd catalyst, rather than decarboxylation reactions [30] or the catalytic reduction of CO_2 to CO via reverse water gas shift in the presence of H_2 [31].

3.2 GC/MS/FID of the produced oils

The composition of the filtered organic liquids (MSO, BSO, and EAP before drying) was analyzed using GC/MS/FID. Final yields of compounds in the n-butanol experiments were calculated involving both BSO and EAP phases. The identification and quantification of the produced oils (more than 88 % of the total area in the chromatograms) revealed the presence of 81 compounds from different families: monomeric phenols, aliphatic acids, alcohols, esters, furans, and ketones. Figure 3 summarizes the total yields (over AS fed) of the compounds derived from lignin and holocellulose decomposition, which were identified and quantified by GC/MS/FID. In general, the production of phenolic monomers when using methanol in the RFC experiments was more significant than the carbohydrate-derived fraction, while the opposite was observed in the n-butanol/water-experiments. More details about the composition of each fraction are given below.

3.2.1 Phenolic monomers

As phenolic monomers are directly produced from the lignin fraction in biomass, Fig. 4 again shows the total yields of phenolic monomers, but now calculated relative to the lignin fraction in AS, which was estimated to be around 34 wt% (Table S1) [22]. Methanol appeared as the best solvent to

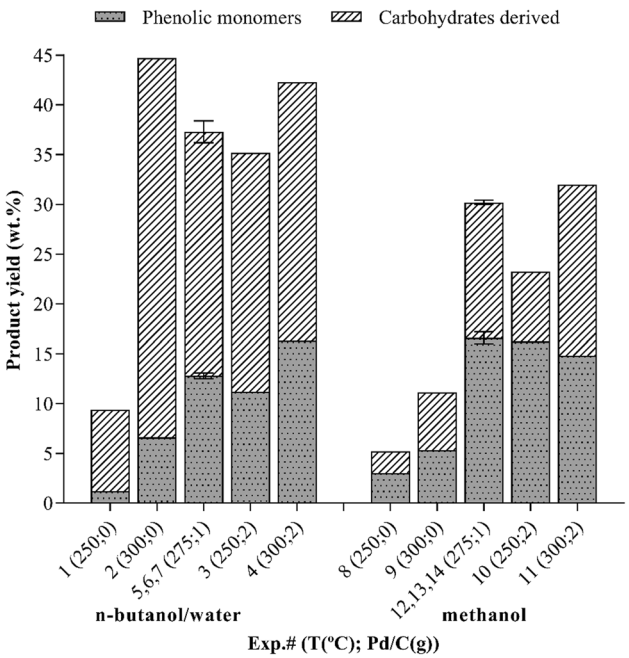

Fig. 3 Production of phenolic monomers and carbohydrates-derived compounds in RCF experiments

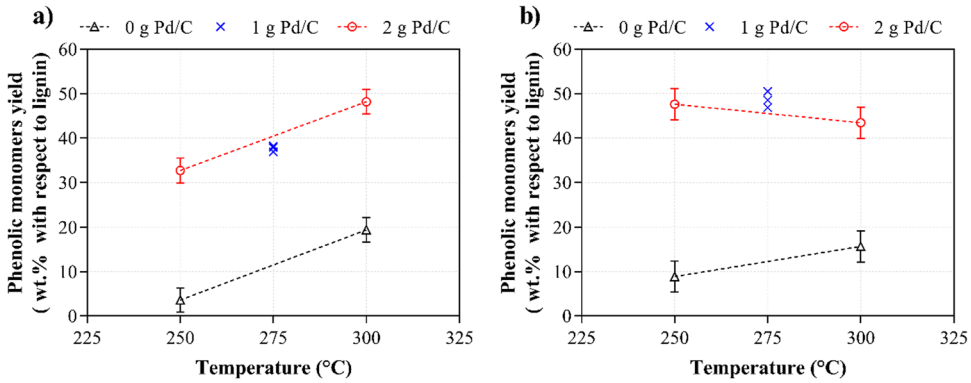

Fig. 4 Effect of the temperature and the catalyst load on the yield of phenolic monomers (wt% over AS lignin): **a** n-butanol/water-experiments; **b** methanol-experiments

enhance the production of lignin monomers at lower temperatures (250 and 275 °C), while this yield was slightly higher in the n-butanol/water-experiments at 300 °C (up to 48 wt% in the presence of 2 g of Pd/C). For both solvents, the monomer yield was less than 10 wt% in the non-catalytic runs at 250 °C (4 wt% in BSO and 9 wt% in MSO), which means that this temperature was not enough to fractionate the lignin at this relatively short reaction time (2 h). Repolymerization reactions between the unsaturated intermediates (coniferyl and sinapyl alcohols) could also be occurring after the solvolytic β-O-4 bond cleavage [32–34]. The ANOVA results indicate that both the temperature and the Pd/C load were significant factors in the n-butanol/water experiments (Fig. 4a), showing a non-linear effect on the monomers yield. Within the conditions tested, the maximal yield of BSO when using n-butanol/water (48 wt%) was obtained at the highest temperature (300 °C) and with the greatest load of catalyst (2 g), which means more than double that obtained at the same temperature and without catalyst (19 wt% of BSO). In the case of methanol-experiments, no significant changes in the monomers yield were observed when varying the temperature, obtaining the highest yield of 44–49 wt% with either 1 or 2 g of catalyst, which means a five-fold increase, from 9 to 48 wt%, in the monomers yield obtained at 250 °C.

In spite of the lower values of AS conversion obtained when using methanol, the production of monomers from lignin was not negatively affected in this reaction medium, which points to good efficiency and selectivity into lignin fractionation during the solvolytic step of the process. Among other linear alcohols, methanol has been pointed out in the literature as a suitable solvent for lignin depolymerization due to its high polarity and hydrogen bonding ability [35].

To keep such high yields of aromatic monomers, the catalytic hydrogenation/hydrogenolysis of unsaturated intermediates plays a crucial role in avoiding repolymerization/condensation reactions and stabilizing the final products [7]. Renders et al. [2] found that operating under 10–30 bars of H_2, as done in this work (26 bars), allowed keeping high monomers yields. According to Lan and Luterbacher [9], the RCF of hardwood using catalysts supported on activated carbon led to yields of aromatic monomers ranging between 40 and 50 wt% (superior to those supported on metal oxide), which was close to the theoretical yield (calculated with the assumption that only the ether bonds linking the monomers in the lignin polymer could be broken). The empirical calculation reported in the literature [18] supposed that ether bonds in the native lignin could represent between two-thirds to three-fourths of the total linkages; hence, this theoretical maximum yield of monomers (calculated as the square of ether bonds fraction) could range between 45 and 56 wt%. Therefore, the results obtained in this study for the RCF of AS suggest a behavior similar to that of hardwood. In fact, AS chemical characterization is closer to hardwood than softwood (hemicellulose content up to 20 wt%, cellulose content slightly lower than 40 wt%, and lignin content higher than 25 wt% [36]).

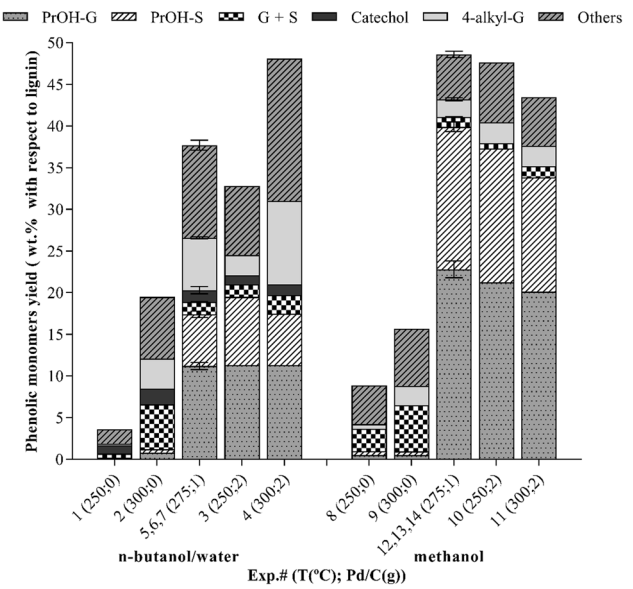

Fig. 5 Mass yields (over AS lignin) of the main phenolic monomers identified in the oils

For further characterization of the lignin-derived fraction, Fig. 5 shows the individual yield (wt% over the amount of lignin in AS) of the main phenolic compounds identified and quantified by GC/MS/FID in the produced oils. More detailed information about the yield data can be found in Table S5 in the SI. Although the same catalyst was employed in both reaction media, the product distribution was strikingly different. In the case of n-butanol/water, the catalytic pathway led to an increased selectivity to 4-n-propanol-guaiacol (PrOH-G) and 4-n-propanolsyringol (PrOH-S), accompanied by the formation of other monomers at lower concentrations, such as guaiacol (G), syringol (S), or catechol. According to the ANOVA analysis, the catalyst load had an apparent positive effect on the yields of PrOH-G and PrOH-S, while the treatment temperature did not significantly affect it. Several studies reported that propanol-substituted syringol and guaiacol are characteristic products of Pd-based catalysts, that tune the OH content of the lignin-derived compounds, concretely the phenolic monomers [2, 17]. Other catalysts such as Ru/C or sulfided NiMo/ɣ-Al_2O_3 tend to favor the generation of the hydrodeoxygenated propyl guaiacol and syringol [17, 29]. Reductive catalytic fractionation can be seen as a combination of two independent processes. Thermal and solvolytic lignin disassembly without altering its native structure is conducted first [37]. Second, the solvent and the catalyst act on aryl ether bonds, primarily on β-O-4 in the so-called metal-catalyzed hydrogenolysis. Indeed, it has been proposed that the mechanism for Ru-catalyzed hydrogenolysis of lignin in methanol catalyzed by Ru/C leading to C3 and C2-fragmented monophenols starts from a nucleophilic attack of methanol on the benzylic position of β-O-4 units of lignin to give α-O-methanol β-O-4 structures and formaldehyde. Ru/C and catalysts play an essential role in the regeneration of methanol from formaldehyde that is produced in transfer hydrogenation from the solvent and on the hydrogenation of the alkenyl side chains [38]; a similar mechanism can be expected for the Pd/C catalyst. Simultaneously, most reactive intermediates in lignin depolymerization, like olefins and carbonyls, which are key in the repolymerization process [39], are stabilized by reductive processes, mainly in the presence of Ru/C [40] or Pd/C [41]. Although both Pd/C and Ru/C are very active in the hydrogenation of olefins, Pd is much less oxophilic than Ru, and hence, Ru/C is far more active in the hydrogenolysis of C-O bonds than Pd/C and therefore, the selectivity of RCF switch to arylpropanols [17].

Scheme S1 shows the different pathways proposed during the lignin solvolysis and hydrogenation/hydrogenolysis of the unstable unsaturated intermediates [2].

The selectivity to PrOH-G and PrOH-S was also considerably increased when operating in methanol. For example, in terms of composition, at 300 °C and a catalyst load of 2 g, PrOH-G and PrOH-S jointly accounted for 78 wt% of the identified monomers (in the methanol-experiments) vs. 36 wt% (in n-butanol/water-experiments). However, non-substituted guaiacol and syringol were mainly observed in the non-catalytic runs. Their production increased with temperature in both reaction media but dropped when the catalyst Pd/C was added. The inverse trend was observed for the presence of alkyl-G compounds (4-methyl, 4-ethyl and 4-propyl guaiacol), which was enhanced in the presence of catalyst, especially in n-butanol/water-experiments. Maximizing PrOH-G and PrOH-S in methanol may likely be related to the direct hydrogenation of the intermediates (direct hydrogenation route in Scheme S1). In contrast, in the case of n-butanol/water-experiments, the important presence of alkyl-G could point to G/S alcohol hydrogenolysis followed by hydrogenation of C_α and C_β bonds (hydrogenolysis plus hydrogenation route in Scheme S1). Finally, it should be mentioned that catechol and phenol were exclusively identified in the oil from n-butanol/water-experiments; in this reaction medium, the production of catechol could be promoted by the presence of water through guaiacol protonation [42–44], while phenol could be produced by deoxygenation of the generated catechol.

3.2.2 Carbohydrate-derived compounds

In addition to the phenolic monomers fraction, the GC/MS/FID analysis of the produced oils revealed the presence of carbohydrate-derived compounds. As these compounds are directly produced from hemicellulose and cellulose fractions in biomass, the production of this type of compounds has been now calculated relative to the holocellulose content in AS, which was estimated to be 57 wt% [22]. These data are shown in Fig. 6. The ANOVA showed that both factors and the interaction between them affect (in a non-linear way) the production of carbohydrate-derived compounds in the methanol reaction medium (Fig. 6b): increasing the temperature in the presence or absence of catalyst was favorable to enhance the holocellulose degradation with a maximal yield of 17 wt% of carbohydrate-derived compounds (at 300 °C and 2 g of Pd/C). However, in the case of n-butanol/water-experiments (Fig. 6a), the temperature only played a significant positive role in the carbohydrate-derived yield when operating in the absence of the Pd/C catalyst, but no significant changes were observed when increasing the temperature in the presence of the catalyst.

As a whole, the conversion of holocellulose into oil was enhanced more in n-butanol/water-experiments than in methanol-experiments, which agrees with the lower unconverted solid yields found in the former reaction medium. However, most of the carbohydrate-derived compounds were not included when calculating the BSO yield (Section 3.1; Figs. 1 and 2c) as part of them was evaporated in the drying stage at the n-butanol evaporation temperature (117 °C) and

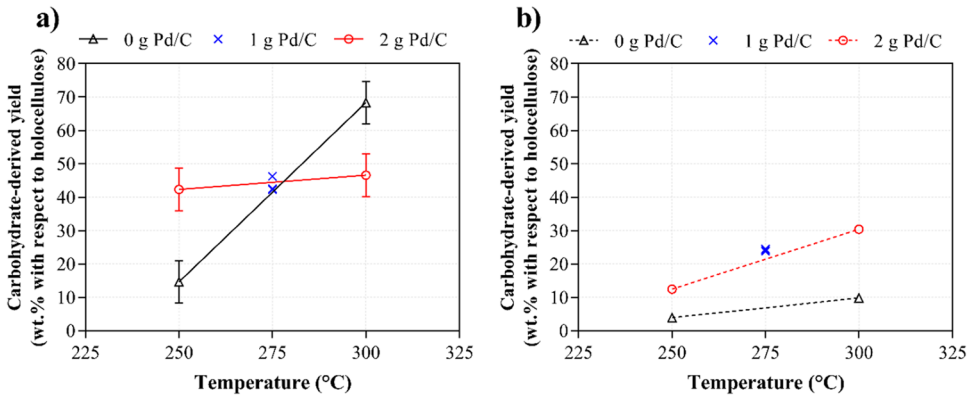

Fig. 6 Effect of temperature and catalyst loading on the yield of the carbohydrate-derived fraction (wt% over AS holocellulose): **a** n-butanol/water-experiments; **b** methanol-experiments

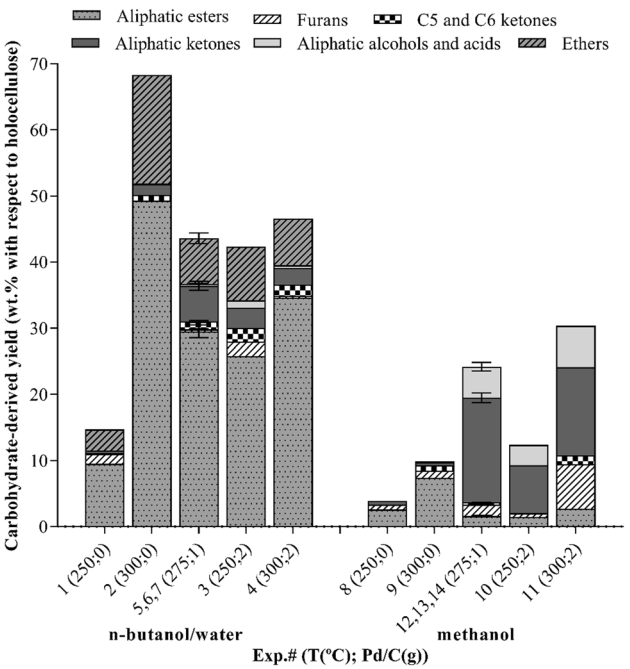

Fig. 7 Mass yields (relative to AS hollocelulose) of the main carbohydrate-derived families identified in the oils

the other part remained in the aqueous phase (RAP before the drying at 105 °C). This fact was confirmed by comparing the GC/MS spectra of the original n-butanol organic phase and the dried BSO (for the GC analysis, BSO was redissolved at the same concentration as the initial solution) (Figure S3 in the SI). These chromatograms showed how the peaks that eluted at relatively low retention times, corresponding to volatile compounds such as acetic acid, butyl ester, 1-hydroxy-2-butanone, butane, 1,1-dibutoxy, only appeared in the original sample, but not in the dried and redissolved sample (BSO).

For further details about the production of carbohydrate derived compounds, Fig. 7 shows how the yields (wt% relative to holocellulose) are distributed into the main chemical families. More detailed information about the individual yields of the main carbohydrate derived compounds can be found in Table S6 in the SI. Aliphatic esters are the most prominent family of compounds detected due to the esterification reactions occurring between the carboxylic acids (mainly acetic acid) released during the holocellulose degradation and the alcohol used as a solvent for RCF (especially for n-butanol/water runs). Carboxylic acid–methyl ester was the major compound when operating in methanol and carboxylic acid–butyl ester in n-butanol/water. The production of these compounds (in terms of mass yield) was more significant in the case of n-butanol/water-experiments. It is evident that the butyl ester branching is heavier than the methyl ester one, thus increasing the weight of this chemical family. However, the lower yield of the carbohydrate-derived fraction found in the methanol reaction medium may also be explained by the reduced conversion of AS (higher yield of unconverted solid) and the remarkable selectivity of methanol to lignin (aromatic) solvolysis. In addition, the noticeable production of ethers in n-butanol/water-experiments, mainly 1,1-di-butoxybutane (Table S6), probably points to a Guerbet condensation and co-condensation of the solvent which is favored in this temperature range (250 to 300 °C) in the presence of H_2 [45]. In the case of methanol-experiments, the aliphatic ketones were the main carbohydrate-derived family, followed by aliphatic alcohols (polyols) and furans coming from hemicellulose processing, especially when the Pd/C catalyst was added.

3.3 Molecular weight distribution of the produced oils

The SEC chromatograms of the BSO and MSO are shown in Fig. 8, while Table 2 summarizes the results in terms of M_n, M_w, and polydispersity (M_w/M_n) of the samples. The operational conditions significantly affected the molecular weight distribution of the produced oils. Generally, comparing the reaction media, lower values of M_w and M_n were obtained when methanol was used, regardless of whether

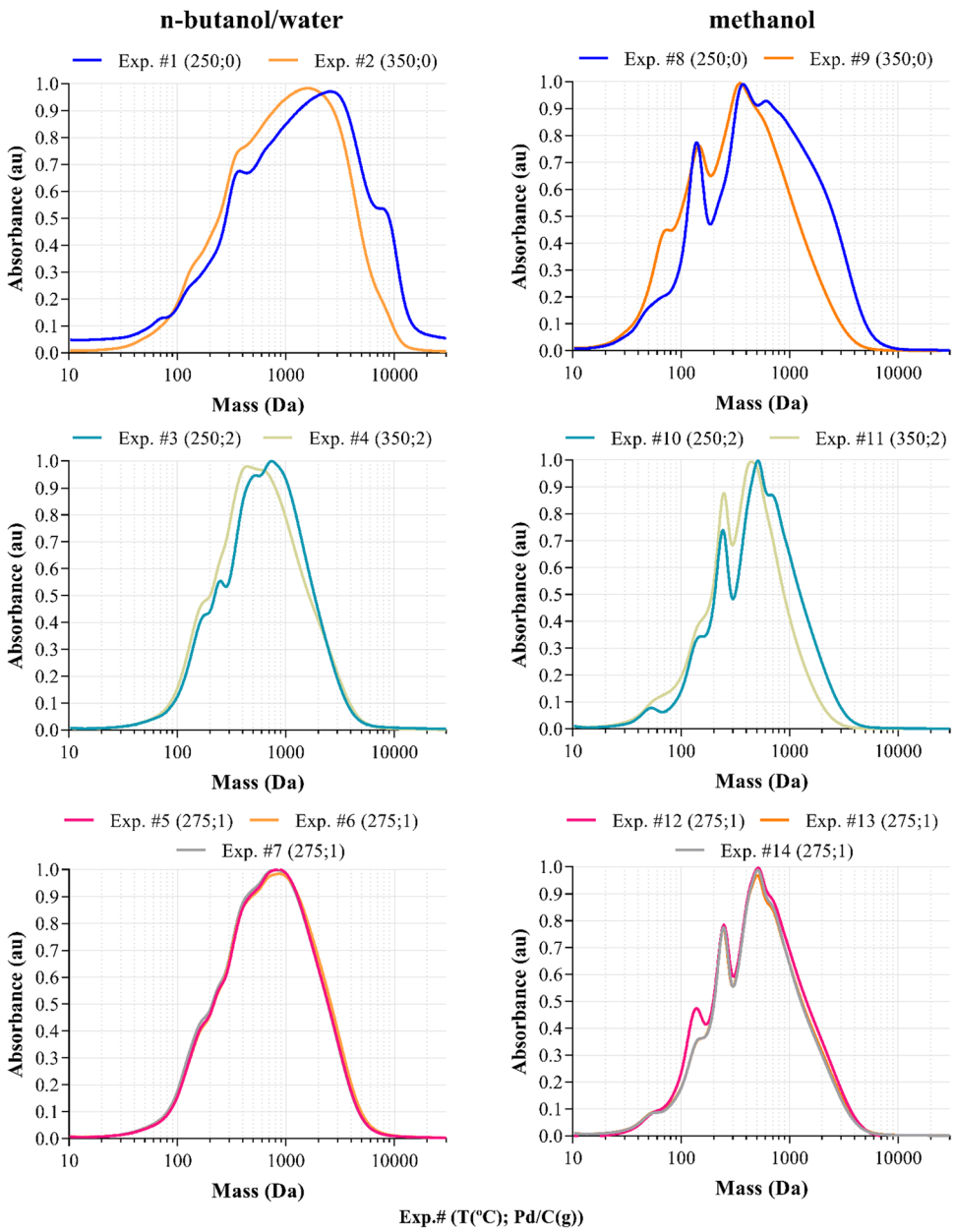

Fig. 8 SEC plots of MSO and BSO

Table 2 Molecular average weights (M_n, M_w, M_w/M_n) of BSO and MSO, using an UV-visible detector

Exp #	Reaction medium	T (°C)	Catalyst load (g)	M_w (Da)	M_n (Da)	M_w/M_n
1	n-butanol/water (1:1 vol.)	250	0	5839	2707	2.2
2		300	0	3132	1576	2.0
3		250	2	1503	847	1.8
4		300	2	1565	802	2.0
5, 6, 7		275	1	1870 ± 56	997 ± 28	1.87 ± 0.01
8	Methanol	250	0	1975	895	2.2
9		300	0	1187	531	2.2
10		250	2	1245	675	1.8
11		300	2	961	501	1.9
12, 13, 14		275	1	1468 ±66	727 ± 13	2.0 ± 0.1

the catalyst was present or not. For example, in non-catalytic conditions and at 250 °C, the M_w of BSO was 5839 Da, but it was almost three times lower (1975 Da) in the case of MSO. The results from the ANOVA of the M_w (Figure S4 in the SI) indicated that the temperature, the catalyst load, and their interaction were significant factors for both reaction media. The M_w of MSO and BSO decreased with the reaction temperature when operating in non-catalytic conditions, but the effect of the temperature turned into non-significant when using 2 g of Pd/C in both reaction media. Furthermore, in methanol-experiments, the effect of using the catalyst was removed by increasing the temperature up to 300 °C.

Figure 8 displays the size exclusion chromatograms of all the produced oils (BSO and MSO) using a UV-detector at $\lambda = 254$ nm that allows ruling out the aliphatic species coming from saccharide or solvent degradation. The plots for BSO (left panels) and MSO (right panels) show different molecular weight distributions. As expected, in the non-catalytic pathway (Exp.#1, 2, 8, 9), the molecular weight distribution is wider and shifted towards higher molecular weights. These data agree with the lower monomers yield obtained via GC/MS/FID in the case of n-butanol/water-experiments (Exp.#1 vs. Exp.#8) and could be explained by repolymerization reactions producing heavy oligomers instead of smaller molecules. The oils produced in the presence of the Pd/C catalyst showed a narrower size distribution and shifted to lower molecular weights, which evidenced the role of the catalyst in the lignin fractionation. It can be observed that the MSO from Exp.#10–14 showed a significant shoulder between 100 and 200 Da and between 200 and 300 Da, which could be related to the high selectivity to PrOH-G (182.2 Da) and PrOH-S (212.2 Da). The effect of the solvent in the catalytic experiments can also be observed in the SEC chromatograms. Thus, when the reactions were run in methanol using Pd/C, the SEC curves of MSO were shifted to lower molecular weights and presented lower average M_n (Table 2) than BSO obtained under the same conditions (675 Da for Exp. # 10 vs. 847 Da for Exp.#3; 727 Da and 997 Da for Exp. #12 and #5). Shoulders in the range of 100–200 Da and 200–300 Da were much less significant in BSO than in MSO. In short, the SEC analyses show the efficiency of the Pd/C catalyst in stabilizing the produced aromatic monomers and preventing condensation reactions in both media, but this effect was more pronounced when methanol was used as a solvent.

3.4 NMR analysis of the produced oils

Diffusion-ordered NMR spectroscopy (DOSY-NMR) can be extremely useful in estimating the molecular weight in depolymerization reaction mixtures [27, 46]. The most important feature of DOSY spectroscopy is that any chemical shift in the ^{1}H NMR spectrum can be directly correlated with the diffusion coefficient of the corresponding molecule. The diffusion coefficient is directly associated with the hydrodynamic radius of the molecule via the Stokes-Einstein equation [47] and, consequently, with its molecular weight [48]. The DOSY-NMR spectroscopy can be therefore seen as a pseudo-SEC technique that allows the estimation of the masses according to their chemical structure. Average diffusion coefficients were obtained for different regions of all the spectra using the integral values for different regions (7.16 to 6.01 ppm for the aromatic region, 3.91 to 3.51 ppm for the methoxy and the saccharide region, whereas the aliphatic region was divided into two intervals, 2.40–1.80 ppm and 1.73–0.72 ppm). The calibration of the diffusion coefficient of polystyrene (PS) and polyethylene glycol and monomeric phenols (PEGP) standards and their corresponding molecular weights was performed [27, 46]. This calibration was successfully used to determine the masses of the aromatic and aliphatic fractions arising from lignin depolymerization. As previously reported, the calibration made with PS standards provided higher accuracy for higher apparent masses, thus corresponding to more hydrophobic oligomers, whereas values calculated with PEGP standards were more suitable for low molecular weight and, therefore, more polar fragments [27]. The average apparent masses estimated by DOSY-NMR using the two different calibration curves are gathered in Table 3.

The average apparent masses for the aromatic region calculated using the PS calibration did not match perfectly in the case of Exp.#1 and #2 with those determined by SEC, although a much better match was achieved for the rest of the experiments. It is noteworthy that the apparent masses for the aromatic region estimated using DOSY are lower than those determined by SEC using RID (Table 3), which may be due to species that are not considered upon integration as, for instance, some oligosaccharides, for which the presence of lower diffusion coefficient species has been detected. Overall, a similar trend can be observed in the apparent mass determined either by DOSY or by SEC.

For BSO samples, the apparent mass (by DOSY) for the aromatic fraction decreased when increasing the temperature in non-catalytic conditions (1080 vs.725 Da for Exp.#1 and #2, respectively). The catalyst load had an apparent positive effect on the depolymerization, as adding 2 g of Pd/C at 300 °C caused a decrease from 725 to 447 Da (Exp.#2 vs. Exp.#4) in the aromatic fraction. A similar effect was observed when 2 g of Pd/C was added at 250 °C, with a decrease in the apparent mass from 1080 to 589 Da (Exp.#1 vs. Exp.#3).

DOSY spectra (Figs. 9 and 10) also provided valuable information about the composition of the different fractions and the formation of reaction products derived from other side reactions than lignin depolymerization. The calculated apparent masses for the first calibration (using

Table 3 Estimated apparent masses using DOSY for the aromatic, methoxy, and aliphatic regions using PS for calibration

Exp.#	Reaction medium	T (°C)	Catalyst load (g)	Mn (Da)*	PS calibration				PEGP calibration			
					Aromatic region[a]	Methoxy region[b]	Aliphatic region[c]	Aliphatic region 2[d]	Aromatic region[a]	Methoxy region[b]	Aliphatic region[c]	Aliphatic region 2[d]
1	n-butanol/water (1:1 vol.)	250	0	1797	1080	1320	604	426	801	1001	419	284
2		300	0	1379	725	1008	435	410	514	741	290	272
3		250	2	763	589	663	n.d	430	407	465	n.d	287
4		300	2	716	447	520	317	397	300	354	204	262
5, 6, 7		275	1	870	595	706	433	495	412	498	289	335
8	Methanol	250	0	813	646	503	363	392	451	342	238	259
9		300	0	566	462	403	323	295	311	267	144	188
10		250	2	629	549	539	363	423	377	369	237	282
11		300	2	505	492	474	249	316	333	320	156	203
12, 13,14		275	1	625	470	457	308	361	317	307	198	236

n.d not detected

*SEC (RID detector)

[a]from 7.16 to 6.01 ppm

[b]from 3.91 to 3.51 ppm

[c]from 2.40 to 1.85 ppm

[d]from 1.72 to 0.72 ppm

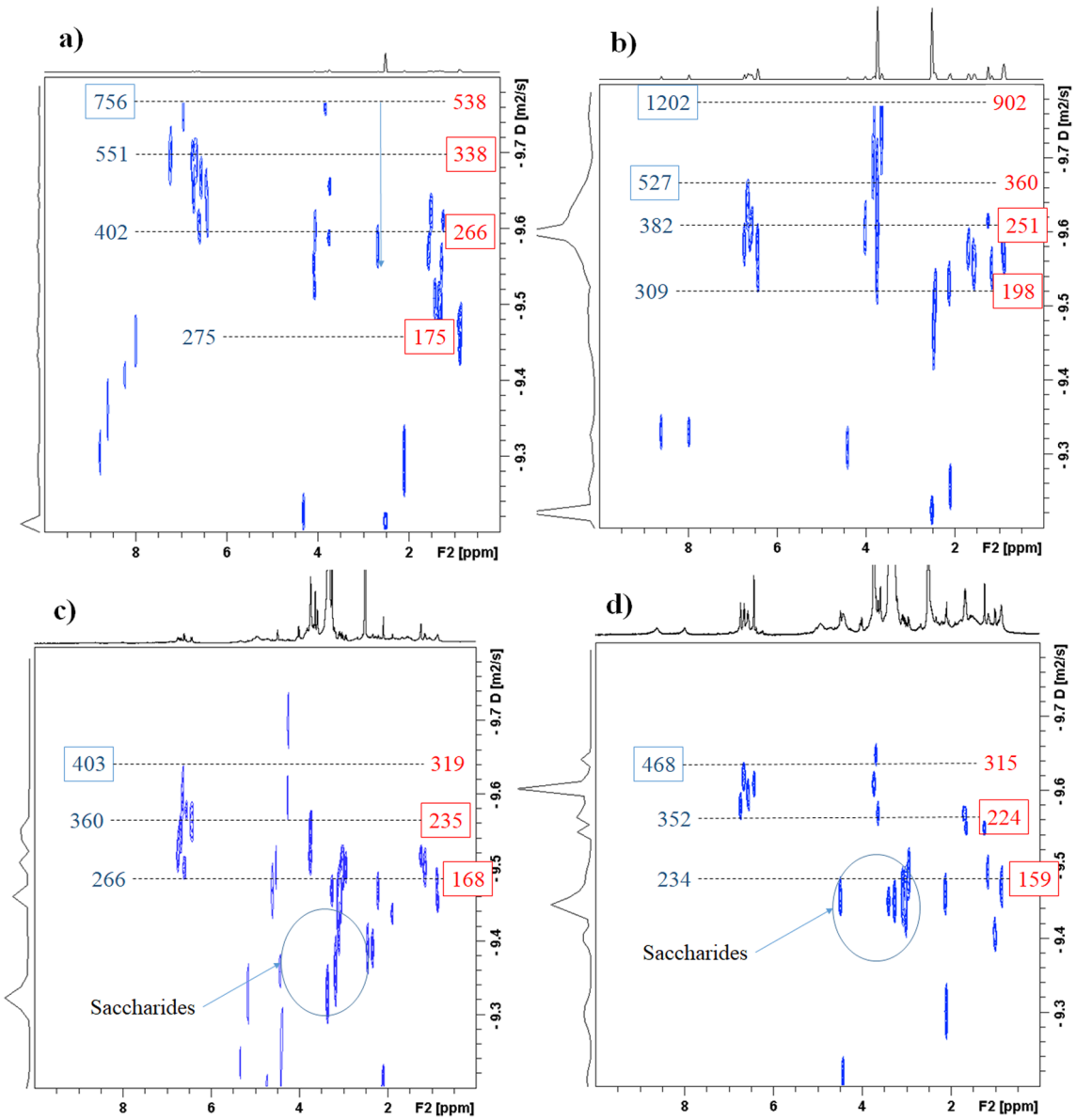

Fig. 9 ^{1}H-DOSY NMR spectra of oils obtained at 300 °C: **a** Exp.#2, BSO without Pd/C; **b** Exp.#4, BSO with Pd/C; **c** Exp.#9, MSO without Pd/C; and **d** Exp.#11, MSO with Pd/C. Red and blue numbers correspond to molecular weights obtained with PEGP and PS calibration, respectively. The numbers in the boxes represent the selected value according to the corresponding calibration

PS standards) can be seen on the left side of the DOSY spectra (blue numbers), and the second calibration (using PEGP standards) is shown on the right side (red numbers). The most accurate mass is in the blue or red square, considering the mass and the calibration curve. DOSY spectra of the BSO samples obtained at 300 °C without or with catalyst (Fig. 9a and b) show that most of the aromatic fractions from RCF reaction carried out at 300 °C without catalyst (Exp.#2) could be found in mass ranges between 266 and 756 Da. In contrast, when the reaction was performed at the same temperature with the catalyst (2 g), the aromatic masses ranged from 198 to 527 Da, evidencing the positive effect of the catalyst in the depolymerization of lignin.

On the other hand, for MSO samples, the effect of Pd/C load was less important. The apparent masses ranged between 462 and 646 Da in all experiments, whatever the reaction conditions (Table 3), which corroborates the results obtained by SEC for this reaction medium. DOSY spectra of the MSO produced with and without catalyst at 300 °C (Exp.#9 and Exp.#11; Fig. 9c and d) presented diffusion traces in the aromatic region ranging from 170 to 470 Da in both cases, showing that the effect of the catalyst was not important in the average apparent mass when using

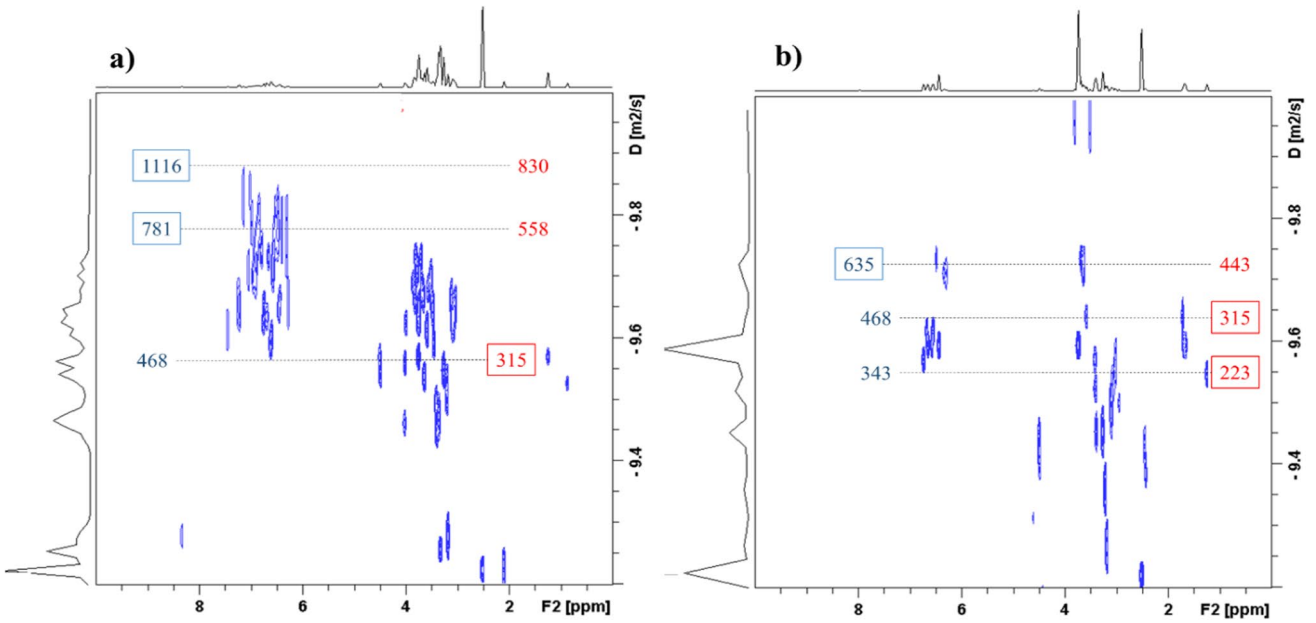

Fig. 10 ^{1}H-DOSY NMR spectra of MSO obtained at 250 °C: **a** Exp. #8, without Pd/C and **b** Exp. #10, with Pd/C

methanol at high temperatures, although it could also be observed that the size distribution was narrower when the catalyst was used. However, the effect of the catalyst was of paramount importance in the apparent masses when the experiment was run at 250 °C (Exp.#8, no catalyst, Exp. #10, 2 g Pd/C; Fig. 10). Thus, when the reaction was run in the absence of catalyst, apparent masses ranged from 315 to 1116 Da (Fig. 10a), while in the presence of catalyst, the apparent masses were in the 223–635 Da range (Fig. 10b).

Concerning the carbohydrate-derived compounds, as can also be observed in Fig. 9a and b (for BSO), the intense diffusion traces present in the aliphatic region (0.7–2.0 ppm) corresponded to apparent masses ranging from 175 to 266 Da in Exp.#2 and from 198 to 250 Da in Exp.#4. Therefore, the apparent mass for the aliphatic compounds was noticeably lower than for the aromatic region in the non-catalytic reaction, for example, in Exp.#2. This means that most of these aliphatics may come from side reactions of n-butanol such as the Guerbet reaction or directly from saccharide degradation products, giving rise to aliphatic esters and ethers, as was pointed out previously ("Carbohydrate-derived compounds"). A similar observation can be made for Exp.#4 (at 300 °C with 2 g of Pd/C), but the difference in the estimated apparent mass was much lower in this case. In addition, the diffusion traces of the aliphatic compounds (Fig. 9b) presented similar masses to those in the aromatic region, which agrees with the significant presence of 4-alkyl-G or PrOH-G and PrOH-S units in the reaction mixture (see Fig. 5); these aliphatic compounds may correspond to the propanol units of the PrOH-G and PrOH-S monomers. DOSY spectra for MSO obtained in the absence or presence of Pd/C (Fig. 9c and d) presented, diffusion traces in the aliphatic region with similar apparent masses as in the aromatic region, showing that some aliphatic chains were connected to the aromatic compounds, although other aliphatic traces presented lower apparent masses than the corresponding aromatic region, as in the MSO sample of Exp.#11.

Besides the diffusion traces corresponding to the methoxy moiety at 3.75 ppm, in all the experiments carried out in methanol (Exp.#8–12), diffusion traces can be observed in the range of 3.0 to 5.5 ppm. These traces could correspond to saccharides, which was confirmed by the traces at 4.5 ppm, which may correspond to the anomeric carbon with the same diffusion coefficient (Figs. 9c, d and 10). These diffusion traces attributed to saccharides were not observed in the DOSY spectra of BSO (Fig. 9a and b), which could be explained by the retention of these saccharides in the aqueous phase separated in the earlier step of the process or because of the drying process at 117 °C.

MSO and BSO samples were analyzed using HSQC-NMR. The main difference between these samples was the presence of intense cross signals (δ_H-δ_C) at 4.49–99.97 ppm, 4.24–101.75 ppm and 4.01–104.55 ppm in the HSQC spectra of MSO samples (Fig. 11a) that were hardly detected in BSO samples (Figs. 11b and 12a). The HSQC-TOCSY spectroscopy allowed unequivocally assigning these signals to anomeric carbon atoms as they presented a strong correlation with signals at 3.21 and 3.11 ppm, evidencing the presence of such saccharides or phenyl glycosides as pointed out in the literature (see Fig. 13a for Exp.#12) [49]. The most intense cross-signal in the aliphatic region of the HSQC spectra (Fig. 11a) corresponded in all cases to the methoxy

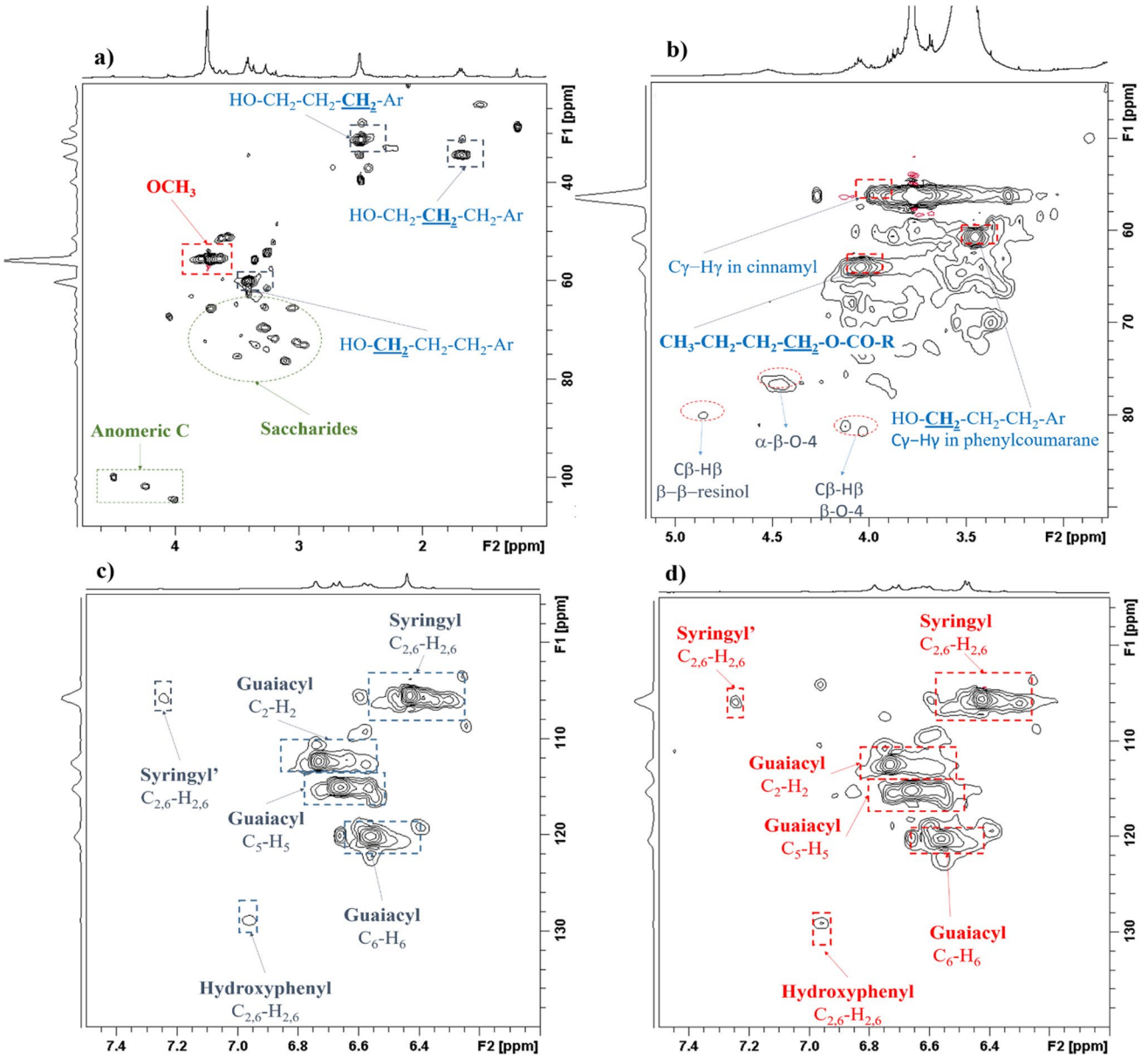

Fig. 11 HSQC spectra in the aliphatic region of oils obtained at 275 °C, 1 g Pd/C: **a** Exp. #12, MSO; **b** Exp. #5, BSO; and HSQC spectra in the aromatic region of oils obtained at 275 °C, 1 g Pd/C: **c** Exp. #12, MSO; **d** Exp. #5, BSO. Syringyl', oxidized syringyl unit

moiety (3.71–55.6 ppm). Besides this signal, HSQC contour at 4.03–63.2 ppm in BSO samples presented a noticeable intensity (Fig. 11b). The HSQC-TOCSY showed that this cross-signal correlated well with three alkyl signals, and therefore, these signals were assigned to butyl esters, produced upon the esterification reactions occurring between the carboxylic acids (mainly acetic acid) released during the holocellulose degradation and the degraded butanol solvent. Additionally, three signals presented remarkable intensity (3.41–60.1 ppm, 2.50–31.1 ppm, and 1.68–34.41 ppm). The HSQC-TOCSY spectroscopy could assign them to the propyl chains presented in PrOH-G and PrOH-S. Concerning the aromatic region, HSQC contours corresponding to guaiacyl, syringyl, and hydroxyphenyl units could be detected as the main signals in all the experiments (Fig. 11c and d), showing very similar patterns for BSO and MSO samples (related with the raw material used), and assigned according to literature data [50, 51].

It has been shown that extrapolated time-zero ^{13}C-HSQC ($HSQC_0$) enables simultaneous quantification and identification of chemicals in metabolite mixtures [52], and recently, $HSQC_0$ has proven to be a reliable methodology for the quantitative analysis of lignin using HSQC [53]. The $HSQC_0$ was carried out for both BSO and MSO (Table S7 in the

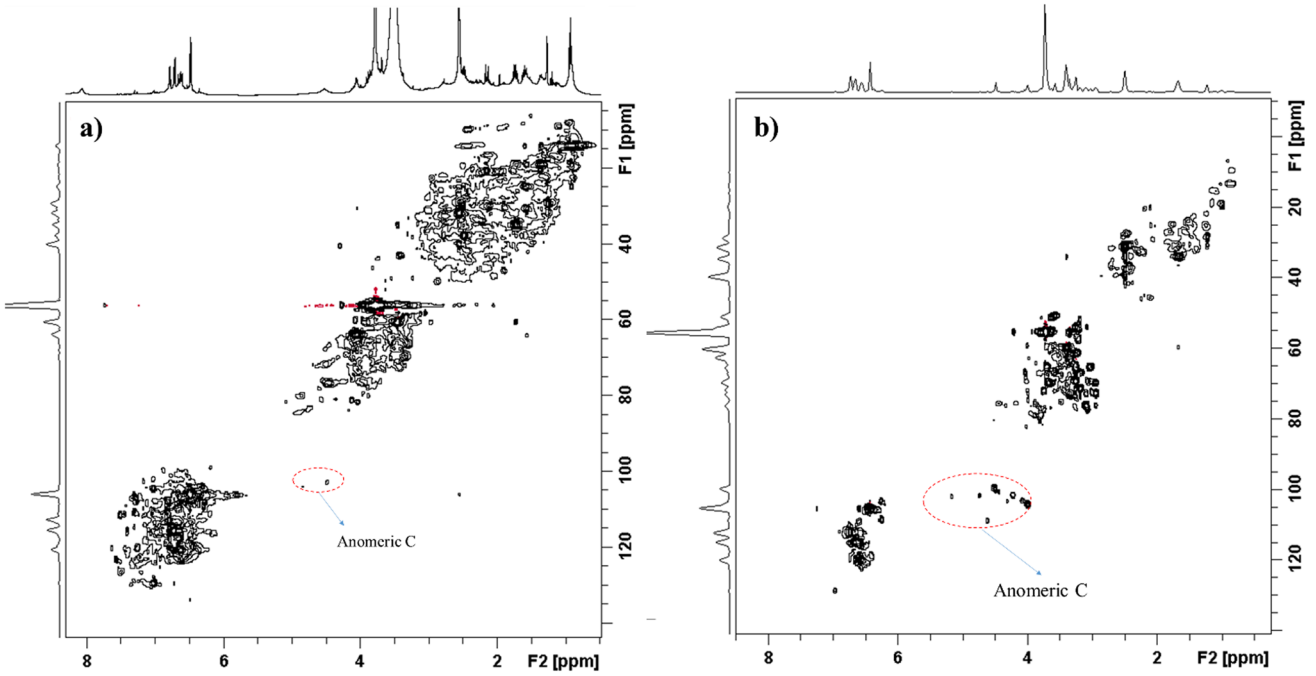

Fig. 12 HSQC spectra for the samples obtained in **a** Exp. #5 (BSO at 275 °C; 1 g Pd/C) and **b** Exp. #11 (MSO at 300 °C; 2 g Pd/C)

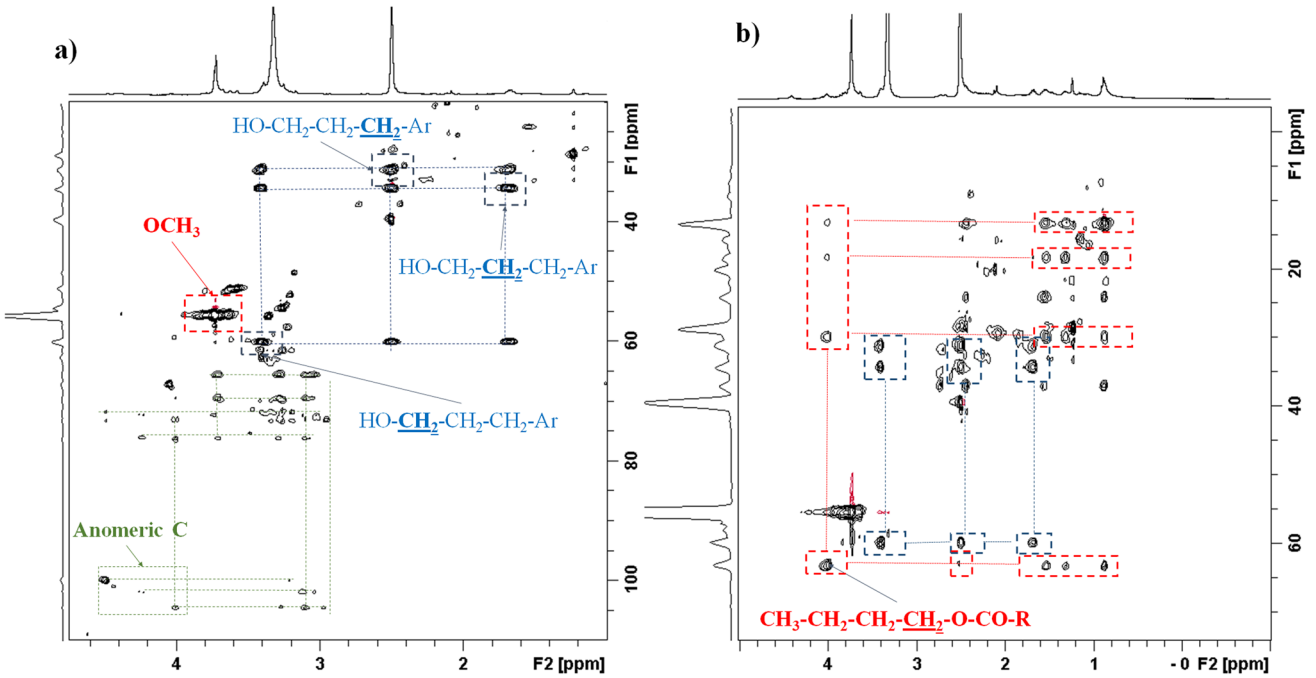

Fig. 13 HSQC-TOCSY in the aliphatic region of oils obtained at 275 °C, 1 g Pd/C: **a** Exp.#12, MSO; **b** Exp.#5, BSO

SI) using the integration of the HSQC contours cited in the literature [50, 51]. Regarding the relative composition of the aromatics, syringyl and guaiacyl units presented similar amounts in both BSO and MSO, with a slight increase in syringyl units in methanol-experiments (50 % in MSO vs. 44 % in BSO). Finally, even if the signals corresponding to the inter-unit linkages presented low intensity, it was tried to evaluate the amount of the most common linkages, phenylcoumarane, resinol, and β-O-4. More noticeable differences were found in the inter-unit linkages. On average, 64

% of these linkages corresponded to β-O-4 moieties in the BSO mixtures, whereas only 55 % were found in the MSO, which could confirm the higher efficiency of methanol in the hydrogenolysis process of β-O-4 linkages, as was also evidenced by the results of the other characterization methods (SEC and GC/MS/FID).

The ^{31}P NMR of the MSO and BSO samples provided valuable information about their content on hydroxy groups (Table 4; Fig. 14). It was observed that the overall number of hydroxy groups was noticeably higher in the MSO samples (6.2–7.8 mmol/g) than in the BSO samples (2.9–5.3 mmol/g) obtained for all the reaction conditions, being the main difference in the content of aliphatic hydroxy groups, that was much higher in the MSO samples (0.6–1.9 mmol/g for BSO vs. 3.8–5.9 mmol/g in MSO). The presence of saccharides in the MSO, evidenced by the DOSY and HSQC spectroscopies, was the origin of this much higher amount of hydroxy groups in the MSO samples. It could also be deduced that some of these aliphatic groups corresponded to PrOH-S and PrOH-G. Indeed, the content in alkyl hydroxy groups in the MSO increased with the reaction temperature regardless of the catalyst presence (4.5–4.7 mmol/g for reactions at 250 °C and 5.9 mmol/g when the reaction was run at 300 °C). However, the amount of PrOH-G and PrOH-S was almost constant in catalytic reactions, which evidences that the increase in aliphatic hydroxy groups was related

Table 4 Estimated hydroxy groups in the MSO and BSO

Exp. NO.	Reaction medium	T (°C)	Catalyst load (g)	Total OH/g	Aromatic OH (mmol/g)	Aliphatic OH (mmol/g)	S/G
1	n-butanol/water (1:1 vol.)	250	0	3.2	2.2	1.1	1.0
2		300	0	2.9	2.3	0.6	0.9
3		250	2	5.3	3.4	1.9	1.4
4		300	2	4.9	3.9	1.0	1.6
5, 6, 7		275	1	4.4	3.2	1.1	1.6
8	Methanol	250	0	6.2	1.8	4.5	1.5
9		300	0	7.6	1.8	5.9	1.1
10		250	2	7.1	2.4	4.7	0.8
11		300	2	7.8	1.9	5.9	1.0
12, 13, 14		275	1	6.2	2.5	3.8	0.8

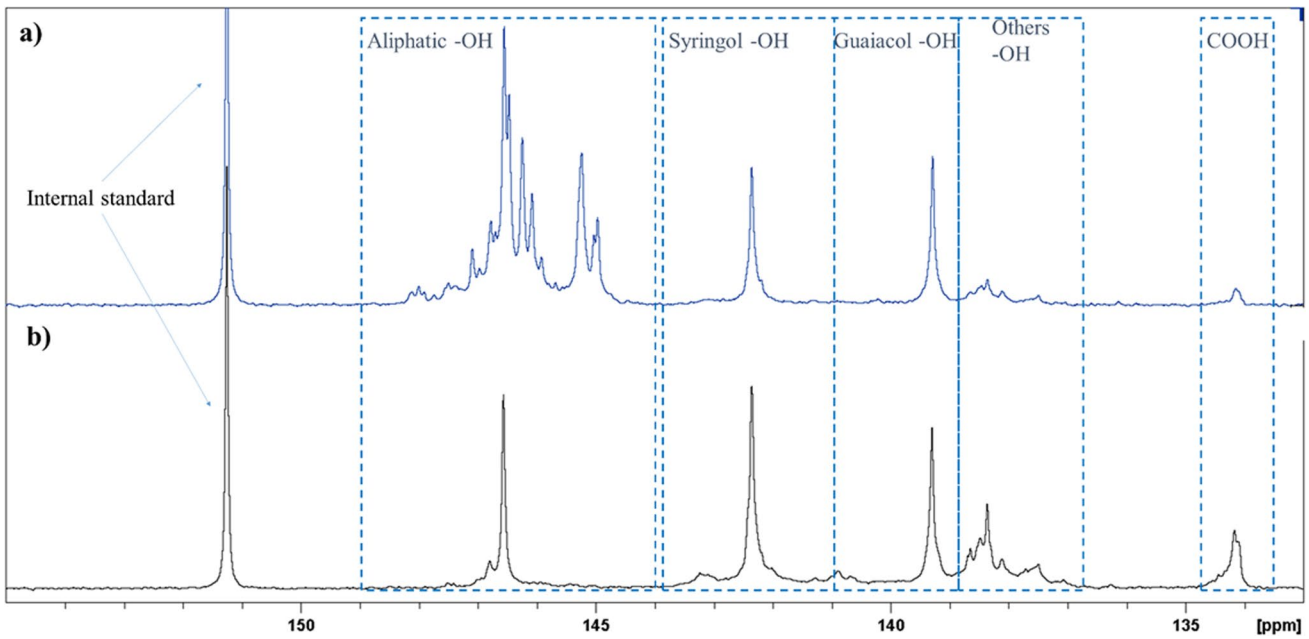

Fig. 14 ^{31}P NMR after derivatization with TMDP of the samples obtained in **a** Exp. #11: (MSO at 275 °C; 1 g Pd/C) and b Exp. #4 (BSO at 300 °C; 2 g Pd/C)

to more efficient solvolysis of the holocellulose fraction at higher temperatures. Aliphatic hydroxy groups in the BSO samples can be mostly ascribed to the presence of propanol side chains. Concerning the aromatic hydroxy groups, the effect of the catalyst was clearly evidenced in the BSO samples, whose content of aromatic hydroxy groups was noticeably higher in the experiments run in the presence of catalyst either at 250 °C (Exp. #1, 2.2 mmol/g; Exp.#3, 3.4 mmol/g) or 300 °C (Exp.#2, 2.3 mmol/g; Exp.#4, 3.9 mmol/g). A similar trend was observed in the MSO samples, in which the presence of the aromatic hydroxy group was higher when the reaction was run in the presence of Pd/C at 250 °C (1.8 mmol/g for Exp.#8 vs. 2.4 mmol/g for Exp.#10), whereas it remained constant at 300 °C (up to 1.9 mmol/g). On the other hand, the content of aromatic hydroxy groups was remarkably higher in the BSO samples, which could be related to the enhanced formation of catechol because of the presence of water in the reaction media.

4 Conclusions

The potential of AS as feedstock in RCF was studied. The type of solvent, the catalyst load, and the temperature significantly impacted the product distribution and characteristics. Less solid (3 to 21 wt%) was obtained when using n-butanol/water as solvent compared to the use of methanol (11 to 67 wt%).

The production of lignin-derived oil was enhanced in the presence of the Pd/C catalyst, obtaining a yield of phenolic monomers up to 49 wt% over the lignin content when using methanol as reaction medium and up to 48 wt% when using the mixture n-butanol/water. Methanol performance was better regarding the selectivity (4-n-propanolguaiacol and 4-n-propanolsyringol) and lower molecular weights (narrower size distributions and lower values of Mw).

The different characterization techniques point to the efficiency of the Pd/C catalyst in stabilizing the produced aromatic monomers and preventing repolymerization reactions.

Supplementary information

Supplementary information section for this work can be found in the online version of the paper:

- Ultimate and proximate analyses, HHV and chemical composition of AS (Table S1); Operating and method parameters of GC/MS/FID analysis (Table S2); Response factor from GC/FID calibration curves and values of the effective carbon number (Table S3); Composition of gases from RCF experiments (Table S4); Yields of the main phenolic compounds identified in the produced oils (Table S5); Yields of the carbohydrate-derived compounds identified in the produced oils (Table S6); Quantitative $HSQC_0$ of the produced oils (Table S7).
- Lignin depolymerization mechanism to phenolic monomers (Scheme S1) Experimental setup for RCF experiments (Figure S1); Filtration setup (Figure S2); GC/MS spectrum of BSO before drying and BSO redissolved in n-butanol (Figure S3); Effect of temperature and catalyst loading on the weight-average molecular weight of the produced oils (Figure S4).

Acknowledgements The authors express gratitude to *Agencia Estatal de Investigación* in Spain (Project PID2020-114936RB-I00), Aragón Government (Research Group Ref. T22_23R), and Navarra Government (Project 'PC177-178 Reducenano 2.0') for providing frame support for this work. A. C. wants to thank M. Angulo (Servicio de RMN at the University of Seville) for the helpful discussion.

Author contribution Zainab Afailal: methodology, investigation, writing-original draft, and editing. Noemí Gil-Lalaguna: methodology, writing-reviewing and editing. Martin Høj: reviewing and editing. Alfonso Cornejo: analyses, writing-reviewing and editing. José Luis Sánchez: reviewing, editing, supervision and funding acquisition. Anker Degn Jensen: reviewing, editing, supervision and project administration.

Funding Open Access funding provided thanks to the CRUE-CSIC agreement with Springer Nature.

Data availability Supporting information is available in the additional files, and further supporting data is available from the authors on request.

Declarations

Ethical approval Not applicable

Competing interests The authors declare no competing interests.

References

1. Abu-Omar MM, Barta K, Beckham GT, Luterbacher JS, Ralph J, Rinaldi R, Román-Leshkov Y, Samec JSM, Sels BF, Wang F (2021) Guidelines for performing lignin-first biorefining. Energy Environ Sci 14(1):262–292. https://doi.org/10.1039/d0ee02870c

2. Renders T, Cooreman E, Van den Bosch S, Schutyser W, Koelewijn SF, Vangeel T, Deneyer A, Van den Bossche G, Courtin CM, Sels BF (2018) Catalytic lignocellulose biorefining in n-butanol/water: a one-pot approach toward phenolics, polyols, and cellulose. Green Chem 20(20):4607–4619. https://doi.org/10.1039/c8gc01031e
3. Renders T, Van den Bosch S, Koelewijn SF, Schutyser W, Sels BF (2017) Lignin-first biomass fractionation: the advent of active stabilisation strategies. Energy Environ Sci 10(7):1551–1557. https://doi.org/10.1039/c7ee01298e
4. Gillet S, Aguedo M, Petitjean L, Morais ARC, da Costa Lopes AM, Łukasik RM, Anastas PT (2017) Lignin transformations for high value applications: towards targeted modifications using green chemistry. Green Chem 19(18):4200–4233. https://doi.org/10.1039/c7gc01479a
5. Ma Z, Kasipandi S, Wen Z, Yu L, Cui K, Chen H, Li Y (2021) Highly efficient fractionation of corn stover into lignin monomers and cellulose-rich pulp over H2WO4. Appl Catal B Environ 284:119731. https://doi.org/10.1016/j.apcatb.2020.119731
6. Pan Z, Li Y, Zhang Z, Xu F, Ramaswamy S, Abdulkhani A, Zhang X (2022) Fractionation of light-colored lignin via lignin-first strategy and enhancement of cellulose saccharification towards biomass valorization. Ind Crop Prod 186:115173. https://doi.org/10.1016/j.indcrop.2022.115173
7. Van den Bosch S, Renders T, Kennis S, Koelewijn SF, Van den Bossche G, Vangeel T, Deneyer A, Depuydt D, Courtin CM, Thevelein JM, Schutyser W, Sels BF (2017) Integrating lignin valorization and bio-ethanol production: on the role of Ni-Al2O3 catalyst pellets during lignin-first fractionation. Green Chem 19(14):3313–3326. https://doi.org/10.1039/c7gc01324h
8. Sturgeon MR, Kim S, Lawrence K, Paton RS, Chmely SC, Nimlos M, Foust TD, Beckham GT (2014) A mechanistic investigation of acid-catalyzed cleavage of aryl-ether linkages: implications for lignin depolymerization in acidic environments. ACS Sustain Chem Eng 2(3):472–485. https://doi.org/10.1021/sc400384w
9. Lan W, Luterbacher JS (2019) Preventing lignin condensation to facilitate aromatic monomer production. Chimia 73(7-8):591. https://doi.org/10.2533/chimia.2019.591
10. Labauze H, Cachet N, Benjelloun-Mlayah B (2022) Acid-based organosolv lignin extraction from wheat straw: kinetic and structural analysis. Ind Crop Prod 187:115328. https://doi.org/10.1016/j.indcrop.2022.115328
11. Schutyser W, Renders T, Van den Bosch S, Koelewijn SF, Beckham GT, Sels BF (2018) Chemicals from lignin: an interplay of lignocellulose fractionation, depolymerisation, and upgrading. Chem Soc Rev 47(3):852–908. https://doi.org/10.1039/c7cs00566k
12. Rinaldi R, Jastrzebski R, Clough MT, Ralph J, Kennema M, Bruijnincx PCA, Weckhuysen BM (2016) Paving the way for lignin valorisation: recent advances in bioengineering, biorefining and catalysis. Angew Chem Int Ed Engl 55(29):8164–8215. https://doi.org/10.1002/anie.201510351
13. Ferrini P, Rinaldi R (2014) Catalytic biorefining of plant biomass to non-pyrolytic lignin bio-oil and carbohydrates through hydrogen transfer reactions. Angew Chem Int Ed 53(33):8634–8639. https://doi.org/10.1002/anie.201403747
14. Ferrini P, Chesi C, Parkin N, Rinaldi R (2017) Effect of methanol in controlling defunctionalization of the propyl side chain of phenolics from catalytic upstream biorefining. Faraday Discuss 202:403–413. https://doi.org/10.1039/c7fd00069c
15. Anderson EM, Katahira R, Reed M, Resch MG, Karp EM, Beckham GT, Román-Leshkov Y (2016) Reductive catalytic fractionation of corn stover lignin. ACS Sustain Chem Eng 4(12):6940–6950. https://doi.org/10.1021/acssuschemeng.6b01858
16. Brienza F, Van Aelst K, Devred F, Magnin D, Sels BF, Gerin PA, Cybulska I, Debecker DP (2022) Reductive catalytic fractionation of wheat straw biomass. ACS Sustain Chem Eng. https://doi.org/10.1021/acssuschemeng.2c02012
17. Van den Bosch S, Schutyser W, Koelewijn SF, Renders T, Courtin CM, Sels BF (2015) Tuning the lignin oil OH-content with Ru and Pd catalysts during lignin hydrogenolysis on birch wood. Chem Commun 51(67):13158–13161. https://doi.org/10.1039/c5cc04025f
18. Yan N, Zhao C, Dyson PJ, Wang C, Liu L-t, Kou Y (2008) Selective degradation of wood lignin over noble-metal catalysts in a two-step process. ChemSusChem 1(7):626–629. https://doi.org/10.1002/cssc.200800080
19. Schutyser W, Van den Bosch S, Renders T, De Boe T, Koelewijn SF, Dewaele A, Ennaert T, Verkinderen O, Goderis B, Courtin CM, Sels BF (2015) Influence of bio-based solvents on the catalytic reductive fractionation of birch wood. Green Chem 17(11):5035–5045. https://doi.org/10.1039/c5gc01442e
20. Feghali E, van de Pas DJ, Parrott AJ, Torr KM (2020) Biobased epoxy thermoset polymers from depolymerized native hardwood lignin. ACS Macro Lett 9(8):1155–1160. https://doi.org/10.1021/acsmacrolett.0c00424
21. Feghali E, Van de Pas DJ, Torr KM (2020) Toward bio-based epoxy thermoset polymers from depolymerized native lignins produced at the pilot scale. Biomacromolecules 21(4):1548–1559. https://doi.org/10.1021/acs.biomac.0c00108
22. Afailal Z, Gil-Lalaguna N, Torrijos MT, Gonzalo A, Arauzo J, Sánchez JL (2021) Antioxidant additives produced from argan shell lignin depolymerization. Energy Fuels. https://doi.org/10.1021/acs.energyfuels.1c01705
23. Dahbi M, Kiso M, Kubota K, Horiba T, Chafik T, Hida K, Matsuyama T, Komaba S (2017) Synthesis of hard carbon from argan shells for Na-ion batteries. J Mater Chem A 5(20):9917–9928. https://doi.org/10.1039/c7ta01394a
24. Chandra T, Zebrowski JP (2016) Hazards associated with laboratory scale hydrogenations. J Chem Health Saf 23(4):16–25. https://doi.org/10.1016/j.jchas.2015.10.019
25. Scanlon JT, Willis DE (1985) Calculation of flame ionization detector relative response factors using the effective carbon number concept. J Chromatogr Sci 23(8):333–340. https://doi.org/10.1093/chromsci/23.8.333
26. Kállai M, Balla J (2002) The effect of molecular structure upon the response of the flame ionization detector. Chromatographia 56(5):357–360. https://doi.org/10.1007/bf02491945
27. Cornejo A, García-Yoldi Í, Alegria-Dallo I, Galilea-Gonzalo R, Hablich K, Sánchez D, Otazu E, Funcia I, Gil MJ, Martínez-Merino V (2020) Systematic diffusion-ordered spectroscopy for the selective determination of molecular weight in real lignins and fractions arising from base-catalyzed depolymerization reaction mixtures. ACS Sustain Chem Eng 8(23):8638–8647. https://doi.org/10.1021/acssuschemeng.0c01375
28. Fulmer GR, Miller AJM, Sherden NH, Gottlieb HE, Nudelman A, Stoltz BM, Bercaw JE, Goldberg KI (2010) NMR chemical shifts of trace impurities: common laboratory solvents, organics, and gases in deuterated solvents relevant to the organometallic chemist. Organometallics 29(9):2176–2179. https://doi.org/10.1021/om100106e
29. Parto SG, Jørgensen EK, Christensen JM, Pedersen LS, Larsen DB, Duus JØ, Jensen AD (2020) Solvent assisted catalytic conversion of beech wood and organosolv lignin over NiMo/γ-Al2O3. Sustain Energy Fuels 4(4):1844–1854. https://doi.org/10.1039/c9se00375d
30. Deng F, Huang J, Ember EE, Achterhold K, Dierolf M, Jentys A, Liu Y, Pfeiffer F, Lercher JA (2021) On the mechanism of catalytic decarboxylation of carboxylic acids on carbon-supported

palladium hydride. ACS Catal 11(23):14625–14634. https://doi.org/10.1021/acscatal.1c03869
31. Zhu M, Ge Q, Zhu X (2020) Catalytic reduction of CO_2 to CO via reverse water gas shift reaction: recent advances in the design of active and selective supported metal catalysts. Trans Tianjin Univ 26(3):172–187. https://doi.org/10.1007/s12209-020-00246-8
32. Erdocia X, Prado R, Corcuera MÁ, Labidi J (2014) Base catalyzed depolymerization of lignin: influence of organosolv lignin nature. Biomass Bioenergy 66:379–386. https://doi.org/10.1016/j.biombioe.2014.03.021
33. Toledano A, Serrano L, Labidi J (2012) Organosolv lignin depolymerization with different base catalysts. J Chem Technol Biotechnol 87(11):1593–1599. https://doi.org/10.1002/jctb.3799
34. Kumaniaev I, Subbotina E, Sävmarker J, Larhed M, Galkin MV, Samec JSM (2017) Lignin depolymerization to monophenolic compounds in a flow-through system. Green Chem 19(24):5767–5771. https://doi.org/10.1039/c7gc02731a
35. Kouris PD, van Osch DJGP, Cremers GJW, Boot MD, Hensen EJM (2020) Mild thermolytic solvolysis of technical lignins in polar organic solvents to a crude lignin oil. Sustain Energy Fuels 4(12):6212–6226. https://doi.org/10.1039/d0se01016b
36. Roger M, Rowell RP, Tshabalala MA (2012) In: Rowell RM (ed) Cell wall chemistry. In Handbook of wood chemistry and wood composites. CRC Press
37. Dao Thi H, Van Aelst K, Van den Bosch S, Katahira R, Beckham GT, Sels BF, Van Geem KM (2022) Identification and quantification of lignin monomers and oligomers from reductive catalytic fractionation of pine wood with GC × GC – FID/MS. Green Chem 24(1):191–206. https://doi.org/10.1039/d1gc03822b
38. Li H, Song G (2019) Ru-catalyzed hydrogenolysis of lignin: base-dependent tunability of monomeric phenols and mechanistic study. ACS Catal 9(5):4054–4064. https://doi.org/10.1021/acscatal.9b00556
39. Kramarenko A, Etit D, Laudadio G, D'Angelo FN (2021) β-zeolite-assisted lignin-first fractionation in a flow-through reactor**. ChemSusChem 14(18):3838–3849. https://doi.org/10.1002/cssc.202101157
40. Van den Bosch S, Schutyser W, Vanholme R, Driessen T, Koelewijn SF, Renders T, De Meester B, Huijgen WJJ, Dehaen W, Courtin CM, Lagrain B, Boerjan W, Sels BF (2015) Reductive lignocellulose fractionation into soluble lignin-derived phenolic monomers and dimers and processable carbohydrate pulps. Energy Environ Sci 8(6):1748–1763. https://doi.org/10.1039/c5ee00204d
41. Zhang K, Li H, Xiao L-P, Wang B, Sun R-C, Song G (2019) Sequential utilization of bamboo biomass through reductive catalytic fractionation of lignin. Bioresour Technol 285:121335. https://doi.org/10.1016/j.biortech.2019.121335
42. Cui K, Yang L, Ma Z, Yan F, Wu K, Sang Y, Chen H, Li Y (2017) Selective conversion of guaiacol to substituted alkylphenols in supercritical ethanol over MoO_3. Appl Catal B Environ 219:592–602. https://doi.org/10.1016/j.apcatb.2017.08.009
43. Yang L, Zhou W, Seshan K, Li Y (2013) Green and efficient synthesis route of catechol from guaiacol. J Mol Catal A Chem 368-369:61–65. https://doi.org/10.1016/j.molcata.2012.11.024
44. Wahyudiono KT, Sasaki M, Goto M (2007) Decomposition of a lignin model compound under hydrothermal conditions. Chem Eng Technol 30(8):1113–1122. https://doi.org/10.1002/ceat.200700066
45. Larina OV, Valihura KV, Kyriienko PI, Vlasenko NV, Balakin DY, Khalakhan I, Čendak T, Soloviev SO, Orlyk SM (2019) Successive vapour phase Guerbet condensation of ethanol and 1-butanol over Mg-Al oxide catalysts in a flow reactor. Appl Catal A Gen 588:117265. https://doi.org/10.1016/j.apcata.2019.117265
46. Cornejo A, Bimbela F, Moreira R, Hablich K, García-Yoldi Í, Maisterra M, Portugal A, Gandía LM, Martínez-Merino V (2020) Production of aromatic compounds by catalytic depolymerization of technical and downstream biorefinery lignins. Biomolecules 10(9):1338. https://doi.org/10.3390/biom10091338
47. Li D, Kagan G, Hopson R, Williard PG (2009) Formula weight prediction by internal reference diffusion-ordered NMR spectroscopy (DOSY). J Am Chem Soc 131(15):5627–5634. https://doi.org/10.1021/ja810154u
48. Pu Y, Cao S, Ragauskas AJ (2011) Application of quantitative 31P NMR in biomass lignin and biofuel precursors characterization. Energy Environ Sci 4(9):3154–3166. https://doi.org/10.1039/c1ee01201k
49. Rencoret J, Marques G, Gutiérrez A, Nieto L, Santos JI, Jiménez-Barbero J, Martínez ÁT, Río JC (2009) HSQC-NMR analysis of lignin in woody (Eucalyptus globulus and Picea abies) and non-woody (Agave sisalana) ball-milled plant materials at the gel state. Holzforschung 63(6):691–698. https://doi.org/10.1515/HF.2009.070
50. Wen J-L, Sun S-L, Xue B-L, Sun R-C (2013) Recent advances in characterization of lignin polymer by solution-state nuclear magnetic resonance (NMR) Methodology. Materials 6(1):359–391
51. Hu G, Cateto C, Pu Y, Samuel R, Ragauskas AJ (2012) Structural characterization of switchgrass lignin after ethanol organosolv pretreatment. Energy Fuel 26(1):740–745. https://doi.org/10.1021/ef201477p
52. Hu K, Westler WM, Markley JL (2011) Simultaneous quantification and identification of individual chemicals in metabolite mixtures by two-dimensional extrapolated time-zero 1H−13C HSQC (HSQC0). J Am Chem Soc 133(6):1662–1665. https://doi.org/10.1021/ja1095304
53. Sette M, Lange H, Crestini C (2013) Quantitative HSQC analyses of lignin: a practical comparison. Comput Struct Biotechnol J 6(7):e201303016. https://doi.org/10.5936/csbj.201303016